**RAPID COMMUNICATION**

# Estimation of far-field wavefront error of tilt-to-length distortion coupling in space-based gravitational wave detection

Ya-Zheng Tao(陶雅正)[1], Hong-Bo Jin(金洪波)[2,3,5,†], and Yue-Liang Wu(吴岳良)[3,4,5]

[1] *The School of Physical Sciences, University of Chinese Academy of Sciences, Beijing* 100049, *China*
[2] *National Astronomical Observatories, Chinese Academy of Sciences, Beijing* 100101, *China*
[3] *The International Centre for Theoretical Physics Asia-Pacific, University of Chinese Academy of Sciences, Beijing* 100190, *China*
[4] *CAS Key Laboratory of Theoretical Physics, Institute of Theoretical Physics, Chinese Academy of Sciences, Beijing* 100190, *China*
[5] *Hangzhou Institute for Advanced Study, University of Chinese Academy of Sciences, Hangzhou* 310024, *China*

(Received 24 November 2022; revised manuscript received 30 November 2022; accepted manuscript online 8 December 2022)

In space-based gravitational wave detection, the estimation of far-field wavefront error of the distorted beam is the precondition for the noise reduction. Zernike polynomials are used to describe the wavefront error of the transmitted distorted beam. The propagation of a laser beam between two telescope apertures is calculated numerically. Far-field wavefront error is estimated with the absolute height of the peak-to-valley phase deviation between the distorted Gaussian beam and a reference distortion-free Gaussian beam. The results show that the pointing jitter is strongly related to the wavefront error. Furthermore, when the jitter decreases 10 times from 100 nrad to 10 nrad, the wavefront error reduces for more than an order of magnitude. In the analysis of multi-parameter minimization, the minimum of wavefront error tends to $Z$[5,3] Zernike in some parameter ranges. Some Zernikes have a strong correlation with the wavefront error of the received beam. When the aperture diameter increases at $Z$[5,3] Zernike, the wavefront error is not monotonic and has oscillation. Nevertheless, the wavefront error almost remains constant with the arm length increasing from $10^{-1}$ Mkm to $10^{3}$ Mkm. When the arm length decreases for three orders of magnitude from $10^{-1}$ Mkm to $10^{-4}$ Mkm, the wavefront error has only an order of magnitude increasing. In the range of $10^{-4}$ Mkm to $10^{3}$ Mkm, the lowest limit of the wavefront error is from 0.5 fm to 0.015 fm at $Z$[5,3] Zernike and 10 nrad jitter.

**Keywords:** laser optical systems, space mission, gravitational wave

**PACS:** 42.60.–v, 07.87.+v, 04.80.Nn **DOI:** 10.1088/1674-1056/aca9c5

## 1. Introduction

There are 90 events of gravitational wave above 10 Hz detected by the ground-based observatories from LIGO, VIRGO and KAGRA collaborations.[1] The gravitational wave observatory below 1 Hz is a space-based mission matching the longer baseline with the order of $10^6$ km·s apart between the spacecrafts of gravitational wave detection.[2] The less than 10 pm phase of the laser beams is shifted by the gravitational wave linked the spacecrafts, which is sensitive to the gravitational wave sources, such as super massive black hole binaries, the galactic white dwarf binaries, etc.[3,4] For this level of precision, many measurement noises need to be suppressed to enhance the signal to noise ratio of gravitational wave sources. The basic one of the noise sources of the heterodyne interferometry in the spacecrafts, called tilt-to-length (TTL) coupling, is the coupling between an angular jitter of the interfering beams and the path length readout, which brings the extra optical path length into the interferometric measurements.[5] TTL coupling not only affects the phase directly in geometric and non-geometric form, but also couples with wavefront errors.[6] Although the transmitted beam obtains initial wavefront errors before propagation in space, the truncated wavefront has the less errors in the receiver aperture after the propagation over long distances.[7] Thus, the tight requirement on the phase stability of the received wavefront is the precondition of the noise reduction.[8] A detailed estimation of the received wavefront errors should be performed first. Moreover, one of the major noises in ground-based observatories is also relevant to TTL coupling.[9] It is obvious that the lower limit of the received wavefront errors constrains the sensitivity to the detection of the weaker strain gravitational wave sources.

The TTL couplings between the wavefront misalignment and some low-order aberrations of the interfering beams are investigated analytically,[7] which is also extended to higher order modes.[10] Utilizing a Zernike polynomial decomposition of wavefront error, the fast and transparent modeling techniques, that is derived from neglecting a significant number of unimportant terms in the expansions of Zernike polynomials, for the purpose of estimating TTL noise associated with various wavefront errors are introduced in Ref. [11], which indicates that the certain combinations of these Zernikes are capable of producing noise far below the Laser Interferometer Space Antenna (LISA)[4] requirements.[11] The numerical

[†]Corresponding author. E-mail: hbjin@bao.ac.cn

© 2023 Chinese Physical Society and IOP Publishing Ltd 

simulation is used to describe the effect of an aberrated transmitting telescope on the light collected by the receiving telescope with Zernike modes.[12] Via calculations of the wavefront aberrations in the far field, an end-to-end investigation of the measurement noise due to the interaction between the telescope jitters and wavefront aberrations is reported in Ref. [13].

In many papers, the wavefront error is estimated at the given parameters: 2.5 Mkm arm length and 300 mm aperture diameter, etc, which are from LISA configuration. In this paper, we estimate the changes of far-field propagation wavefront error with the arm length, the aperture diameter and the pointing jitter, which are used generally for the gravitational wave detection. We use Nijboer–Zernike Theory[14] to describe the diffraction propagation of the transmitted distorted beam. For the first time, the numerical calculation of the diffraction propagation between two telescope apertures is performed with the Gaussian beam decomposition (GBD)[15] based on the numerical calculations. The numerical calculations are performed using the software package IfoCAD.[16]

The results of this paper show that the consistent wavefront error appears in the different methods between the Hermite–Gaussian modal decomposition[17] and GBD at the same parameters. That justifies the GBD using for the diffraction propagation of laser beam. More informative results indicate that the wavefront error has no significant difference above $10^4$ km, but significant increases below $10^4$ km and is affected remarkably by the aperture diameter and the pointing jitter. With the aperture diameter varying, the wavefront error of the different aperture diameters is not monotonic and has the oscillation.

In Section 2, we introduce the TTL–wavefront distortion coupling and the expression of distortion wavefront. In Section 3, there is detailed description about GBD used for the propagation of the laser beam as the sum of a series of fundamental Gaussian beams. In Section 4, the numerical results are shown. In Section 5, the estimation of the far-field wavefront error is summarized as the conclusion.

## 2. TTL–wavefront distortion coupling and the expression of distortion wavefront

In space-based gravitational wave detection, the ideal transmitted beam propagating into the telescope aperture of another spacecraft (S/C) is described as a truncated Gaussian beam.[17] After the extremely far field propagation, the wavefront of the truncated Gaussian beam is approximated as a spherical wave. Thus, the received top-hat beam has no additional phase shift caused by the jitter of the initial beam, which is shown in the left part of Fig. 1. However, through the local telescope system, the wavefront of the transmitted beam is usually distorted by the various mechanisms. Before being transmitted to another S/C, the wavefront carries errors and is not an ideal beam. After far distance propagation, the shape of the wavefront, which deviates from a spherical wave, is derived from the initial wavefront errors. That is shown in the right part of Fig. 1. Generally, this mechanism is called as TTL–wavefront distortion coupling, i.e., the jitter of transmitter brings the inconstant wavefront with the received one at the receiver. The measurement of a laser beam has the additional phase offset.

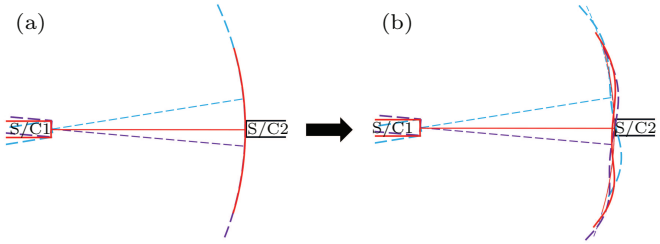



**Fig. 1.** Schematic diagram of how TTL–wavefront distortion coupling occurs. (a) The ideal transmitted beam with the jitter propagating into the telescope aperture of another spacecraft. (b) The propagation of the beam carrying wavefront errors. The truncated wavefront is transformed from the spherical wave (a) to the distorted one (b).

Frits Zernike and Bernard Nijboer developed a diffraction theory, which provides a description of the aberrated complex field in the image plane.[14] Through the aperture of telescope, the electric field is expressed as

$$E_{\rm a}(r;0) = E_0(r;0)\,{\rm e}^{{\rm i}\Omega_{\rm a}}, \tag{1}$$

where $E_0(r;0)$ is the amplitude of an assumed truncated circular Gaussian beam

$$E_0(r;0) = \begin{cases} {\rm e}^{-r^2/w_0^2}, & \text{if } r \le r_{\rm a}, \\ 0, & \text{if } r > r_{\rm a}. \end{cases} \tag{2}$$

The $w_0$ is the waist radius of the Gaussian beam and $r_{\rm a}$ is the aperture radius of the telescope. $\Omega_{\rm a}$ in Eq. (1) is the total phase departure, which is formed by a set of Zernike polynomials

$$\Omega_{\rm a}(\rho,\theta) = \sum_{n=0}^{N}\sum_{m=-n}^{n} c_n^m Z_n^m(\rho,\theta),$$

with

$$Z_n^m(\rho,\theta) = \begin{cases} R_n^m(\rho)\cos(m\theta), & \text{if } m \ge 0, \\ R_n^{-m}(\rho)\sin(-m\theta), & \text{if } m < 0, \end{cases}$$
$$R_n^{|m|}(\rho) = (-1)^{(n-|m|)/2}\rho^{|m|}P_{(n-|m|)/2}^{(|m|,0)}(1-2\rho^2), \tag{3}$$

where $c_n^m$ represents coefficients and $Z_n^m$ are Zernike polynomals written with Noll indexing.[18] $\rho = r/r_{\rm a}$ is restricted to unit disk ($0 \le \rho \le 1$), and $\theta$ is the azimuth. $n-m \ge 0$ and is even. Zernike polynomals $Z_n^m(\rho,\theta)$ are circle polynomials. $R_n^m(\rho)$ are the radial polynomials. $P_k^{(\alpha,\beta)}$ is the Jacobi polynomial of degree $k$. And $R_n^m(\rho)$ satisfies the orthogonality relation

$$\int_0^1 R_n^{|m|}(\rho)R_{n'}^{|m|}(\rho)\rho\,{\rm d}\rho = \frac{\delta_{n,n'}R_n^{|m|}(1)}{2(n+1)}. \tag{4}$$

When the propagation distance is very far for space-based gravitational wave detection, and the pointing jitter of S/C is limited to $10^{-8}$ rad/$\sqrt{\text{Hz}}$ level, the diffraction integral satisfies the conditions for Fraunhofer diffraction

$$E(r,\psi,z) = \frac{\mathrm{e}^{\mathrm{i}kz}\,\mathrm{e}^{\frac{\mathrm{i}k}{2z}r^2}}{\mathrm{i}\lambda z} {r_\mathrm{a}}^2 \times \int_0^1 \int_0^{2\pi} \mathrm{e}^{-\rho^2}\,\mathrm{e}^{\mathrm{i}\Omega_\mathrm{a}(\rho,\theta)}\,\mathrm{e}^{-\mathrm{i}v\rho\cos(\theta-\psi)}\rho\,\mathrm{d}\rho\,\mathrm{d}\theta, \quad (5)$$

where $w_0 = r_\mathrm{a}$ is assumed and $v = r_\mathrm{a} rk/z$.

The expression (5) is computed numerically, which is performed by C++ code in the IfoCAD package.[16]

In Eq. (5), $E(r,\psi,z)$ is expressed as $A(x,y,z)\,\mathrm{e}^{\mathrm{i}\Theta(x,y,z)}$, where $A(x,y,z)$ is the amplitude of $E(r,\psi,z)$ and $\Theta(x,y,z)$ is the phase of the wavefront,

$$E(r,\psi,z) = A(x,y,z)\,\mathrm{e}^{\mathrm{i}\Theta(x,y,z)}, \quad \begin{cases} x = r\cos(\psi), \\ y = r\sin(\psi). \end{cases} \quad (6)$$

The phase difference $\delta\Theta(x,y,z)$ of the wavefront is between the distorted Gaussian beam $E(r,\psi,z)$ and the given reference distortion-free Gaussian beam $E(r,\psi,z)_0$

$$\delta\Theta(x,y,z) = \Theta(x,y,z) - \Theta(x,y,z)_0. \quad (7)$$

## 3. Gaussian beam decomposition

As the mixture of Zernike polynomials increases, expression (5) becomes more complex. Via neglecting a significant number of unimportant terms in the expansions of Zernike polynomials and Hermite–Gaussian modal decomposition based propagation of an approximation in the initial beam, TTL noise associated with various wavefront errors is estimated in Ref. [11]. Furthermore, the beam decomposition methods are required for more conveniently simulating the diffraction of an aberrated or distorted Gaussian beam.

In this paper, the Gaussian beam decomposition (GBD) is used for the beam profile decomposition to compute the diffraction propagation including propagation between the optical components. The basic idea of GBD is to describe the propagation of a beam as the sum of a series of fundamental Gaussian beam propagation. These Gaussian beams are distributed on a grid, also called grid beams. Each grid beam propagates following the ABCD law and has its own intersection point with optical components. Therefore, GBD can also be considered as one kind of "fat rays" tracing. GBD was firstly proposed by Greynolds in 1986,[15] and has been further developed in recent years. The further details of GBD and its computation process can be found in Appendix A. This paper focuses on the diffraction propagation of aberrated Gaussian beam by using GBD. We program C++ code to perform these calculations numerically. The code is included into IfoCAD[16] package for the first time.

**Table 1.** List of the parameters for distorted circular Gaussian beam clipped by a circular aperture centered in the beam waist.

| Parameter | Description | Value |
|---|---|---|
| $\lambda$ | wavelength | 1064 nm |
| $\omega_0$ | beam waist | 150 mm |
| $z_0$ | distance to the waist | 0 |
| $P$ | power | 1 W |
| $ds$ | propagation distance | 2.5 Mkm |
| $r_\mathrm{a}$ | aperture radius | 150 mm |

By means of GBD we can obtain the radial electric field distribution of the transmitted beam at the far field after propagation. We firstly perform the numerical calculations based on the same parameters as in Sasso's work,[7] to verify the validity of the GBD method. These parameters are listed in Table 1. The wavefront error generated randomly is constrained to $\lambda/20$ peak-to-valley deviation from a plane. The radial plane radius of the received beam is determined by the jitter of S/C

$$r = L \cdot a, \quad (8)$$

when $L$ is 2.5 Mkm arm length, and $a$ is 100 nrad jitter, the receiving plane corresponds to a circular plane with 250 m radius. On this plane, we compute the phase difference $\delta\Theta$ between distorted Gaussian beam and a reference distortion-free Gaussian beam with Eq. (7). The peak-to-valley phase difference is calculated by

$$\mathrm{PV} = \frac{|\delta\Theta_\mathrm{Peak}| + |\delta\Theta_\mathrm{Valley}|}{2\pi}\lambda. \quad (9)$$

The best-fit coefficients of Zernike polynomials in expression (3) for the transmitted beam are shown in Table 2. The results of relevant calculation are shown in Fig. 2, where the left is the wavefront error at the transmitter, and the right one is the wavefront error at the receiving plane. It is shown that PV = 14.116 pm is consistent with the result in the paper.[7]

**Table 2.** The best-fit Zernike coefficients of distortion, which come from fitting Zernike polynomials to the wavefront at receiver.

| $Z_n^m$ | $Z_0^0$ | $Z_1^{-1}$ | $Z_1^1$ | $Z_2^{-2}$ | $Z_2^0$ | $Z_2^2$ |
|---|---|---|---|---|---|---|
| $c_n^m$ | 0. | 0. | 0. | 0.0967293 | 0.00795719 | 0.0662892 |
| | $Z_3^{-3}$ | $Z_3^{-1}$ | $Z_3^1$ | $Z_3^3$ | $Z_4^0$ | |
| | 0.0130634 | –0.0565416 | –0.0225312 | 0.0491065 | 0.0164262 | |

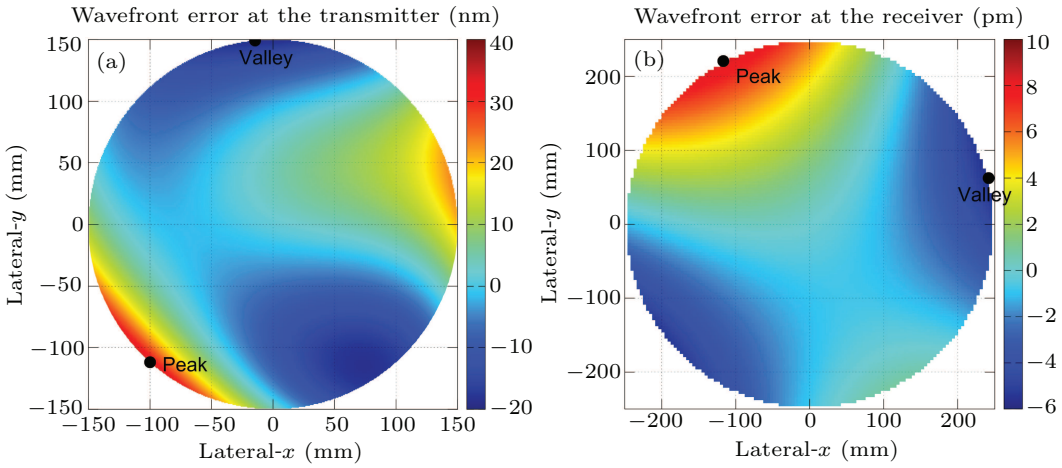



**Fig. 2.** Wavefront at the transmitter (a) and the wavefront error (b) at the receiver. The coefficients of Zernike polynomials for the numerical calculation are listed in Table 2. The transmitted wavefront has $\lambda/20$ peak-to-valley deviation from a plane. The numerical calculated values of peak and valley are 32.9119 nm and −20.2904 nm, respectively. The wavefront error described by PV in the right graph is about 14.1 pm. The numerical calculated values of peak and valley are 8.49655 pm and −5.61987 pm, respectively.

## 4. Numerical results

Based on the given parameters including propagation distances in the context, the numerical calculation of wavefront (WF) error has been verified for consistency. In order to analyze deeply the lower limit of the far-field wavefront error, the different parameters, the arm length, the aperture diameter and the pointing jitter, are also considered.

Firstly, the pointing jitter is chosen as 100 nrad, which is used at LISA configuration. Besides, the invariant parameters are initial wavefront error $\lambda/20$ and aperture diameter 400 mm. The propagation distance expressed as arm length is in the range of $10^{-4}$ Mkm to $10^{3}$ Mkm for space-based gravitational wave detection. The Zernikes $Z_n^m$ are scanned by changing $m$ and $n$ values. Based on the parameters, the far-field wavefront error is calculated by IfoCAD[16] package including GDB method in the context. The numerical results are shown in Fig. 3.

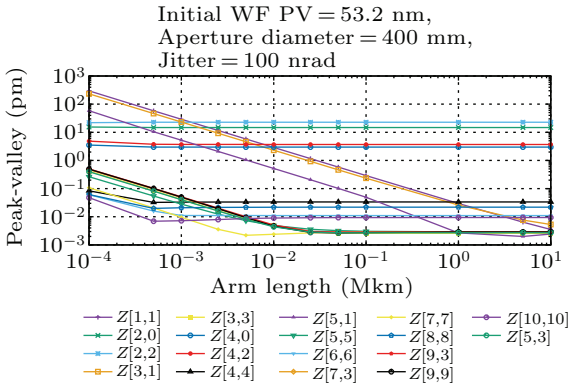



**Fig. 3.** At 100 nrad jitter, PV values of the wavefront error of distorted Gaussian beam at the receiver after propagation, which are relevant to the different Zernikes. The initial wavefront error is constrained to 53.2 nm. The diameter of the telescope aperture is 400 mm.

As shown in Fig. 3, the PV values of wavefront error related to the different Zernikes have the remarkable difference for the several orders of magnitude in picometer. When Zernikes $Z_n^m$ are scanned by changing $m$ and $n$ values, it is found that the main source of wavefront errors is relevant to low-order aberration ($n < 5$) and higher-order aberrations become more obvious in shorter arm lengths than long arm. The lower limit of wavefront error is in the range of 0.1–0.002 pm related to the arm length from $10^{-4}$ Mkm to 10 Mkm.

Secondly, the pointing jitter is changed as 10 nrad, decreased by an order of magnitude. The aperture diameter is chosen as 300 mm. As shown in Fig. 4, with a smaller jitter, the PV values of wavefront error are depressed by 1 to 2 orders of magnitude, covering the whole arm length range. Furthermore, the trend of PV values has not much changes with arm length increasing. In the arm length range of 0.1 Mkm to 10 Mkm, the main sources of wavefront errors are relevant to $Z[2,0]$, $Z[2,\pm2]$, $Z[4,0]$ and $Z[4,\pm2]$, corresponding to defocus, astigmatism, primary spehrical, and 2nd astigmatism, respectively. In this case, the lower limit of wavefront error is from 0.5 fm to 0.015 fm.

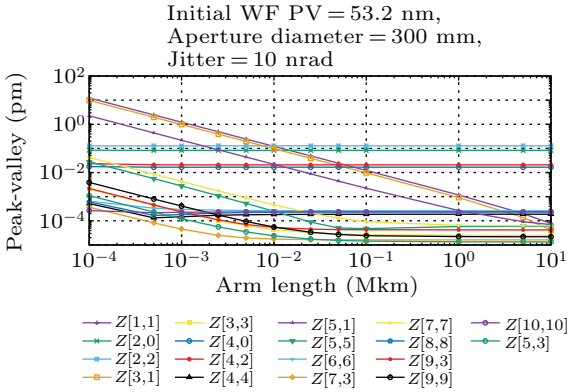



**Fig. 4.** Similar results to Fig. 3 with 10 nrad jitter and 300 mm aperture diameter.

Finally, the effect of different telescope apertures is considered. The aperture diameters vary from 200 mm to 500 mm. The 100 nrad and 10 nrad jitter are both used. Referring to the

results from Figs. 3 and 4, the chosen $Z[5,3]$ is almost relevant to the least PV values of wavefront error among the Zernikes in the arm length range of 0.1 Mkm to 10 Mkm. As shown in Fig. 5, with the aperture diameter increasing, the wavefront error is not monotonic and has the oscillation. Two groups of the broken lines are relevant to the different jitters. The lower lines are relevant to the 10 nrad jitter. The lowest limit of wavefront error is near 0.01 fm consistent with the results in Fig. 4. As an inference, the aperture diameter selection is not easy to be fixed at the range for reducing the wavefront error.

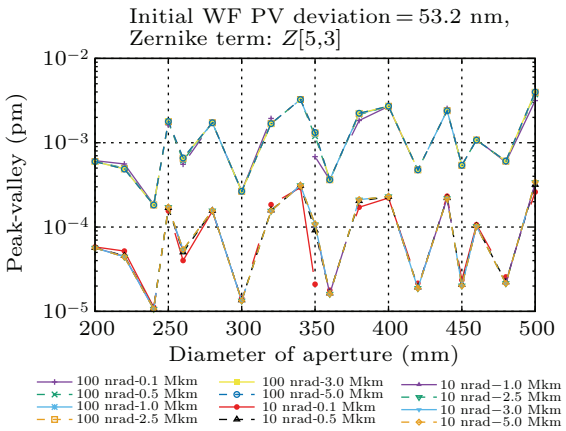



**Fig. 5.** At Zernike $Z[5,3]$, PV values of the wavefront error of propagated beam with the telescope aperture diameter increasing at the transmitter.

When the distance of laser beam propagation is very long, the change of wavefront error is tiny. That result is shown in Fig. 6(a). Two groups of the lines are relevant to the 100 nrad and 10 nrad jitter, respectively. The wavefront error is very slightly increasing in the arm length range of $10^{-1}$ Mkm to $10^3$ Mkm. The different aperture diameters of 240 mm and 500 mm bring an order of magnitude increasing in wavefront error.

The magnitude of the gravitational wave is the strain $h = \delta L/L$ characterized the change of the proper distance between the space–time points. In the heterodyne interferometry, the wavefront plane of the laser beam is like the scale of a ruler to measure the distance. The wavefront error means the scale error of a ruler. Thus, PV/$L$ values have effect on the measured magnitude of gravitational wave. The relation between the best arm length $L$ of S/Cs and the detectable frequency $f_*$ of gravitational wave source is expressed as the transfer frequency $f_* = \frac{C}{2\pi L}$ ($C$ is the light speed).[19] Thus, the change of PV/$L$ with arm length increasing is transformed into the transfer frequency decreasing. These calculations are shown in Fig. 6(b). The upper and lower bounds of PV/$L$ values are relevant to the aperture diameters of 500 mm and 240 mm. As shown in Fig. 6(b), the PV/$L$ values increase with transfer frequency increasing and the lowest limit of PV/$L$ is relevant to the 10 nrad jitter. Thus, as an inference, the decrease of the wavefront error brings the sensitivity to gravitational wave sources increasing.

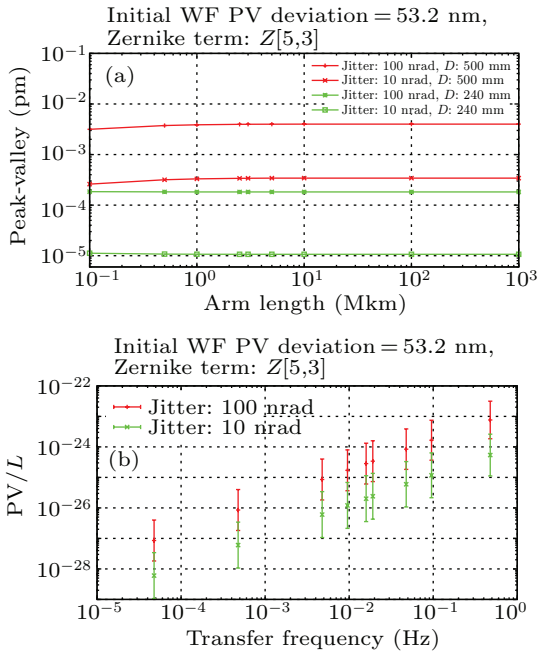



**Fig. 6.** (a) PV values relevant to the arm length from $10^{-1}$ Mkm to $10^3$ Mkm. (b) The calculated PV/$L$ values with the transfer frequency increasing.

## 5. Conclusion

In space-based gravitational wave detection, TTL–wavefront distortion coupling is one of the major noise sources. In the paper, we estimate the wavefront error, which is derived from the transmitted beam being distorted by various mechanisms. The initial wavefront error generated randomly is constrained to $\lambda/20$. Zernike polynomials are used for the description of the aberrated wavefront of the transmitted beam. In the analysis of multi-parameter minimization, the minimum of wavefront error tends to $Z[5,3]$ Zernike in some parameter ranges. Some Zernikes have a strong correlation with the wavefront error of the received beam. By means of Gaussian beam decomposition, we obtain the radial electric field distribution of the transmitted beam at the far field after propagation. The phase difference between the distorted Gaussian beam and a reference distortion-free Gaussian beam is calculated by the peak-to-valley values.

In the paper, the variant parameters, the arm length, the aperture diameter and the pointing jitter, are considered. The pointing jitter is very sensitive to the wavefront error, i.e., 10 times decrease from 100 nrad to 10 nrad brings more than an order of magnitude reduction in the far-field wavefront error. With the aperture diameter varying, the wavefront errors of the different aperture diameters are not monotonic and have the oscillation. It implies that the aperture diameter is not easy to be fixed at the range for reducing the far-field wavefront error. The wavefront error is very slightly increasing

from $10^{-1}$ Mkm to $10^{3}$ Mkm arm length at $Z$[5,3] Zernike and 10 nrad jitter. In the range of $10^{-4}$ Mkm to $10^{3}$ Mkm, the lowest limit of wavefront error changes from 0.5 fm to 0.015 fm at $Z$[5,3] Zernike and 10 nrad jitter. All the results imply that the decrease of the wavefront error brings the increase of the sensitivity to gravitational wave sources.

## Appendix A: Gaussian beam decomposition

The basic idea of GBD is to describe the propagation of a beam as the sum of a series of fundamental Gaussian beams. The propagation of Gaussian beam can be easily computed. Therefore, the implementation of GBD is to find the coefficient of each chosen fundamental Gaussian beam, and superimpose these fundamental beams to reconstruct the electric field. An illustration is shown in Fig. A1.

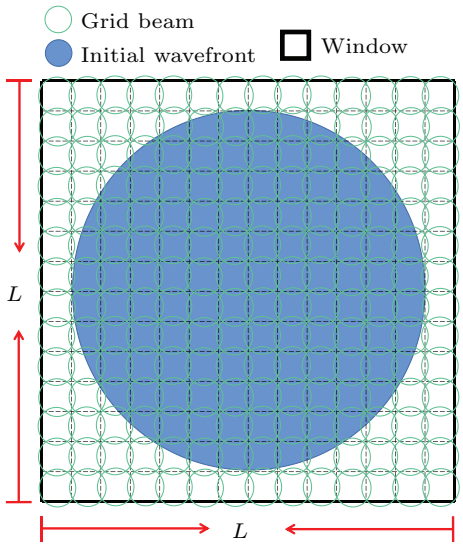



**Fig. A1.** A simple illustration of GBD method. The green one is fundamental grid Gaussian beam, which is arranged in window. The window in the graph is chosen to be square. The blue one is the wavefront to be decomposed.

By taking enough sampling points in space, the problem can be expressed as solving a system of linear equations

$$\boldsymbol{B}\boldsymbol{c} = \boldsymbol{W}_{\mathrm{f}}, \tag{A1}$$

where $\boldsymbol{W}_{\mathrm{f}}$ represents the complex electric field sampled from the wavefront to be decomposed. $\boldsymbol{c}$ is the coefficient vector of fundamental Gaussian beams, and $\boldsymbol{B}$ is the set of $N\times N$ fundamental Gaussian beams in space

$$\boldsymbol{c} = \begin{pmatrix} c_1 \\ c_2 \\ \vdots \\ \vdots \\ c_{N\times N} \end{pmatrix}, \quad \boldsymbol{W}_{\mathrm{f}} = \begin{pmatrix} w_1 \\ w_2 \\ \vdots \\ w_{N\times N} \end{pmatrix}, \tag{A2}$$

$$\boldsymbol{B} = \begin{bmatrix} b_1(\boldsymbol{x}_1) & b_2(\boldsymbol{x}_1) & \cdots & b_{N\times N}(\boldsymbol{x}_1) \\ b_1(\boldsymbol{x}_2) & b_2(\boldsymbol{x}_2) & \cdots & b_{N\times N}(\boldsymbol{x}_2) \\ \vdots & \cdots & \ddots & \vdots \\ b_1(\boldsymbol{x}_{N\times N}) & b_2(\boldsymbol{x}_{N\times N}) & \cdots & b_{N*N}(\boldsymbol{x}_{N\times N}) \end{bmatrix}. \tag{A3}$$

Fundamental Gaussian beams are chosen on a grid of $N\times N$ in the plane area, which is called window. Fundamental Gaussian beams are placed on the center of each grid, also known as grid beams. On the window, there are various options for grid, the simplest being an square. The size of the window should be large enough to cover the entire beam spot, otherwise the decomposition accuracy will be highly affected because of information loss. It should be noted that choosing grid in the plane is not essential, but is a simple and practical way. In Ref. [20], methods of taking grid points were discussed on curved surfaces.

Considering the uniqueness of the solution to the system of matrix linear equations, matrix $\boldsymbol{B}$ should be determined. Therefore the number of space data points $\boldsymbol{x}_i$ should be no less than the number of grid beams $N\times N$. Another relevant parameter for the chosen of grid beams is the waist factor $f_{\mathrm{ws}}$. It determines both the waist of all grid beams and the tightness of the arrangement between grid beams

$$w_{0\mathrm{g}} = \frac{D}{f_{\mathrm{ws}}}, \tag{A4}$$

where $D$ is the interval between two adjacent grid beams, determined by the window size and the grid beam number

$$D = \frac{L}{N}. \tag{A5}$$

In this paper, the relevant parameters of GBD chosen in simulations are all based on Table A1.

**Table A1.** List of the parameters for GBD.

| Parameter | Description | Value |
|---|---|---|
| $n$ | grid number of the GBD | 200×200 |
| $L$ | window size of the GBD | $\frac{8}{3}r_{\mathrm{a}}$ |
| $f_{\mathrm{ws}}$ | waist factor of the GBD | 0.75 |
| $s$ | grid shape of the GBD | square |

## Acknowledgements

We thank Gudrun Wanner from Max Planck Institute for Gravitational Physics (Albert Einstein Institute) for the great contribution to the improvement of the quality of this paper. We thank Yun-Kau Lau for the useful discussions. This work has been supported in part by the National Key Research and Development Program of China (Grant No. 2020YFC2201501), the National Natural Science Foundation of China (Grant No. 12147103, special fund to the center for quanta-to-cosmos theoretical physics) (Grant No. 11821505), the Strategic Priority Research Program of the Chinese Academy of Sciences (Grant No. XDB23030100), and the Chinese Academy of Sciences (CAS). In this paper, the part of the numerical computation is finished by TAIJI Cluster.

## References


[1] The LIGO Scientific Collaboration, the Virgo Collaboration and the KAGRA Collaboration 2021 (Preprint 2111.03606)
[2] Ruan W H, Liu C, Guo Z K, Wu Y L and Cai R G 2020 *Nature Astronomy* **4** 108
[3] Jennrich O 2009 *Classical and Quantum Gravity* **26** 153001
[4] Amaro-Seoane P, Audley H, Babak S, *et al.* 2017 (Preprint 1702.00786)
[5] Schuster S, Wanner G, Tröbs M and Heinzel G 2015 *Applied Optics* **54** 1010
[6] Robertson D, McNamara P, Ward H and Hough J 1997 *Classical and Quantum Gravity* **14** 1575
[7] Sasso C P, Mana G and Mottini S 2018 *Classical and Quantum Gravity* **35** 185013
[8] Thorpe J I 2010 *Classical and Quantum Gravity* **27** 084008
[9] Mueller G 2005 *Opt. Express* **13** 7118 12
[10] Zhao Y, Shen J, Fang C, Liu H, Wang Z and Luo Z 2020 *Opt. Express* **28** 25545
[11] Weaver A J, Mueller G and Fulda P J 2022 *Classical and Quantum Gravity* **39** 195016
[12] Kenny F and Devaney N 2021 *Classical and Quantum Gravity* **38** 035010
[13] Sasso C P, Mana G and Mottini S 2019 *Opt. Express* **27** 16855
[14] Nijboer B R A 1947 *Physica* **13** 605
[15] Greynolds A W 1986 *Propagation of generally astigmatic gaussian beams along skew ray paths Diffraction Phenomena in Optical Engineering Applications* vol. 560 (SPIE) pp. 33–51
[16] Wanner G, Heinzel G, Kochkina E, Mahrdt C, Sheard B S, Schuster S and Danzmann K 2012 *Opt. Commun.* **285** 4831
[17] Saleh B E A and Teich M C 1991 *Beam Optics* (New York: John Wiley & Sons, Inc.) chap 3, pp. 80–107
[18] Noll R J 1976 *J. Opt. Soc. Am.* **66** 207
[19] Prince T A, Tinto M, Larson S L and Armstrong J W 2002 *Phys. Rev. D* **66** 122002
[20] Worku N G, Hambach R and Gross H 2018 *JOSA A* **35** 1091